4-Nitrophenylhydrazone Crystals with Large Quadratic Nonlinear Optical Response by Optimal Molecular Packing

Eun-Young Choi,[‡,†] Pil-Joo Kim,[‡] Mojca Jazbinsek,[§] Jong-Taek Kim,[⊥] Yoon Sup Lee,[⊥] Peter Günter,[§] Soon W. Lee,[∥] and O-Pil Kwon*,[‡]

[‡]Department of Molecular Science and Technology, Ajou University, Suwon 443-749, Korea

[§]Nonlinear Optics Laboratory, ETH Zurich, CH-8093 Zurich, Switzerland

[⊥]Department of Chemistry and School of Molecular Science (BK 21), Korea Advanced Institute of Science and Technology (KAIST), Daejeon 305-701, Korea

[∥]Department of Chemistry (BK21), Sungkyunkwan University, Natural Science Campus, Suwon 440-746, Korea

ABSTRACT: We investigate a novel nonlinear optical nitrophenylhydrazone (NPH) crystal, 3,4,5-trimethoxybenzaldehyde-4-nitrophenylhydrazone (TMO-NPH). Compared with many acentric NPH crystals having rod-shaped heads reported previously, the TMO-NPH molecule maintains the acentric intermolecular hydrogen bond synton through hydrazone and nitro groups but has distinct space filling characteristics due to a different shape of the headgroup, the disk-shaped trimethoxybenzaldehyde. We investigated the crystal structure and its characteristics, as well as details of the microscopic and the macroscopic nonlinear optical properties by quantum chemical calculations using density functional theory (DFT) and powder second-harmonic generation at nonresonant conditions. For comparison, DA-NPH (4-dimethylaminobenzaldehyde-4-nitrophenylhydrazone) having a rod-shaped head and known nonlinear optical properties is also investigated by the same analysis. TMO-NPH crystals have the

Space Filling Characteristics

monoclinic space group symmetry Pn and exhibit a large macroscopic optical nonlinearity due to a favorable molecular packing with a very high order parameter $\cos^3(\theta_p) = 0.90$, while DA-NPH exhibits a lower order parameter $\cos^3(\theta_p) = 0.33$. The diagonal effective hyperpolarizability tensor component of TMO-NPH crystals is 30% higher than the largest tensor component of DA-NPH, even though the microscopic molecular susceptibility of TMO-NPH molecule is only about half of the one of DANPH.
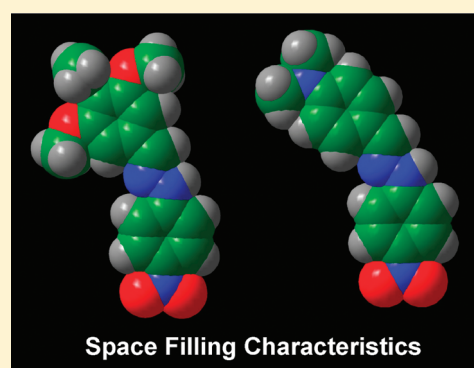
1. INTRODUCTION

Acentric organic crystals[1,2] are useful materials for quadratic nonlinear optical applications such as frequency conversion, terahertz-wave generation, and ultrafast electro-optics.[3] A challenging topic for organic crystals exhibiting a large macroscopic nonlinear optical susceptibility is the molecular design forming noncentrosymmetric molecular packing with a high order parameter in the crystalline state.[2] In organic crystals, molecular packing is mainly influenced by the following two factors: intermolecular interactions and space filling characteristics, that is, functional groups and the shape/size of the constituent molecules. The widely investigated nitrophenylhydrazone (NPH) derivatives exhibit an especially high tendency for forming a noncentrosymmetric molecular order in the crystalline state due to hydrazone and nitro functional groups and non-rod bent shape.[4−8] Main intermolecular interactions of many acentric NPH crystals[4−8] present strong hydrogen bonds between the hydrazone and the nitro group $(-N≡N-H\cdots O-N-)$ with a short distance of about 2.3 Å, which most often leads to a λ-shaped packing.[5]

Although many acentric NPH crystals exhibit a relatively large macroscopic nonlinearity, the molecular ordering in the crystalline state is not optimal for second-order nonlinear optical

applications that require a high diagonal nonlinear susceptibility element, $\chi_{iii}^{(2)}$, such as most often used in electro-optics[1] and terahertz wave generation.[9] For example, DA-NPH (4-dimethylaminobenzaldehyde-4-nitrophenylhydrazone, see Figure 1a) crystals exhibit a very large nonresonant diagonal nonlinear optical susceptibility element, $\chi_{111}^{(2)}(-2\omega,\omega,\omega) = 280$ pm/V, but an even larger off-diagonal element, $\chi_{221}^{(2)}(-2\omega,\omega,\omega) = 320$ pm/V measured at 1.9 μm fundamental wavelength.[4,10] This is because DA-NPH molecules are not aligned perfectly parallel, as shown in Figure 2.[4,10] The reason for such an alignment is, besides hydrogen-bonding interactions, related to the shape of DA-NPH molecules. During crystallization, molecules with a rod-shaped head (dimethylaminobenzaldehyde, see Figure 1a) adopt a bent shape to fill the space with a relatively large angle of more than 90° between the neighboring molecules. A parallel alignment of DA-NPH molecules would potentially increase the diagonal susceptibility element $\chi_{111}^{(2)}$ by a factor of 3, which would be beyond the best value measured to date in organic crystals.[11]
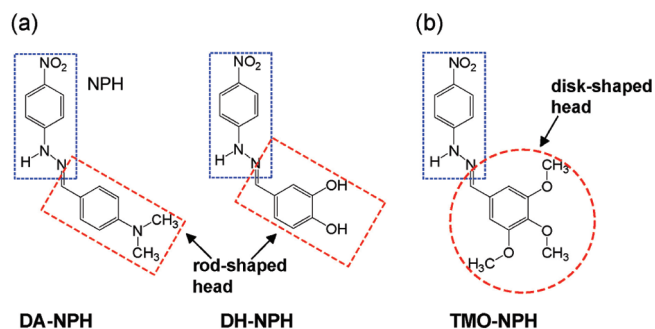
Figure 1. The chemical structure of NPH derivatives having a rod-shaped head (DA-NPH and DH-NPH) (a) and having a disk-shaped head (TMO-NPH) (b).

It is therefore interesting to investigate the possibilities for optimal packing with NPH derivative molecules.

In this work, we investigate a different nitrophenylhydrazone crystal, TMO-NPH (3,4,5-trimethoxybenzaldehyde-4-nitrophenyl-hydrazone), and relate its properties to previously investigated NPH crystals. The TMO-NPH molecule was chosen since it maintains the main supramolecular interactions through hydrazone and nitro groups but introduces a different shape of the head by using a disk-shaped trimethoxybenzaldehyde (see Figure 1b). Although the synthesis and a rough estimation of the macroscopic resonant nonlinearity at a wavelength of 1.3 μm have been previously reported,[12] the crystal structure and its characteristics, as well as a more detailed evaluation of the microscopic and the macroscopic nonlinear optical properties at nonresonant conditions have not been investigated yet. We report on the theoretical analysis by quantum chemical calculations using density functional theory (DFT) and powder second-harmonic generation at the nonresonant wavelength of 1.9 μm to evaluate the microscopic and the macroscopic optical nonlinearities of TMO-NPH crystals. For comparison, DA-NPH with a rod-shaped head and known nonlinear optical properties is also investigated by the same analysis. TMO-NPH crystals have the monoclinic space group symmetry Pn and exhibit a large macroscopic optical nonlinearity with optimal molecular packing for electro-optics and terahertz-wave generation.

2. EXPERIMENTAL SECTION

2.1. Materials. The NPH materials were prepared according to literature,[4,12] and the chemical identification and the purity was determined by ^{1}H NMR and elemental analysis. ^{1}H NMR data were recorded on a Varian 400 MHz. All chemical shifts are reported in ppm (δ) relative to $(CH_3)_4Si$.

2.1.1. 3,4,5-Trimethoxybenzaldehyde-4-nitrophenylhydrazone (TMO-NPH). 3,4,5-Trimethoxy-benzaldehyde (10 g contains >30% water) and 4-nitrophenylhydrazine (10.06 g, 0.05 mol) was dissolved in methanol (300 mL). Acetic acid (20 drops) for catalyst was added dropwise into the solution under N_2 conditions. The solution was heated at 70 °C for 2 days. After the solution was cooled to room temperature, orange-brown powder was filtered and washed with methanol. The products were recrystallized in acetone. Yield: 72%. ^{1}H NMR (400 MHz, DMSO-d_6, δ): 11.40 (s, 1H, CH), 8.23 (d, 2H, J = 8.8, C_6H_4), 8.07 (s, 1H, NH), 7.29 (d, 2H, J = 8.0, C_6H_4), 7.15 (s, 2H, C_6H_2), 3.96 (s, 6H, OMe), 3.81 (s, 3H, OMe). Elemental analysis for $C_{16}H_{17}N_3O_5$: (%) calcd C 58.00, H 12.68, N 5.17; found C 58.08, H 12.69, N 5.16.

2.1.2. 4-Dimethylaminobenzaldehyde-4-nitrophenylhydrazone (DA-NPH). ^{1}H NMR (400 MHz, DMSO-d_6, δ): 11.05 (s, 1H, CH),
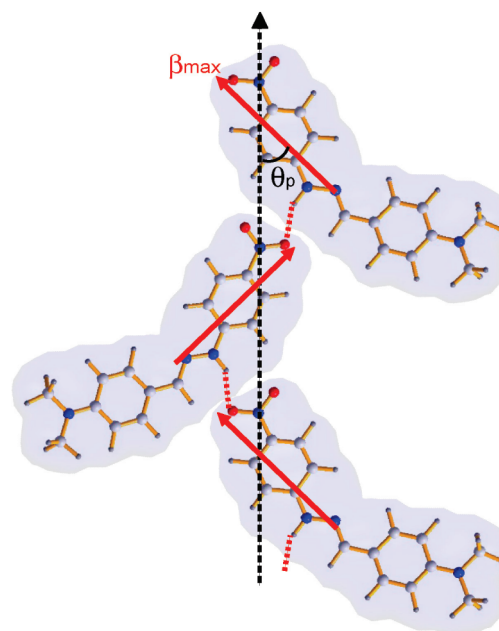
Figure 2. The λ-shaped molecular packing of the DA-NPH crystal. The main hydrogen bonds between the N—H···O—N groups are illustrated with the dotted lines. The solid and the dotted vectors present the direction of the maximum first hyperpolarizability, β_{max}, as determined by finite-field calculations and the polar axis of the crystal, respectively. The angle between the polar axis of the crystal and the hyperpolarizabilities β_{max} of the molecules is $\theta_p \approx 46.6°$.

8.09 (d, 2H, J = 9.2, C_6H_4), 7.93 (s, 1H, NH), 7.54 (d, 2H, J = 8.8, C_6H_4), 7.09 (d, 2H, J = 8.0, C_6H_4), 6.74 (d, 2H, J = 8.8, C_6H_4), 2.96 (s, 6H, N(CH$_3$)$_2$). Elemental analysis for $C_{15}H_{16}N_4O_2$: (%) calcd C 63.37, H 5.67, N 19.71, O 11.25; found C 63.31, H 5.64, N 19.72.

2.2. Single-Crystal Structure. *2.2.1. TMO-NPH.* $C_{16}H_{17}N_3O_5$, M_r = 331.33, monoclinic space group Pn (point group m), a = 4.0325(7) Å, b = 12.6155(17) Å, c = 15.365(2) Å, β = 97.535(9)°, V = 774.9(2) Å^3, Z = 2, μ = 0.107 mm^{-1}, D_c=1.420 mg/m^3, crystal size 0.740 × 0.540 × 0.360 mm^3, $F(000)$ = 348. Of the 9761 reflections collected in the Θ range of 2.10° to 28.32° on a Bruker CCD diffractometer, 3317 were unique reflections (R_{int} = 0.1805, completeness = 95%). The structure was solved by the direct methods using SHELXTL package of crystallographic software[13] and refined by the full-matrix least-squares technique on F^2, 285 variables; the final R_1= 0.0670, wR_2 = 0.1799 for F_o^2 > $2\sigma(F_o^2)$ and R_1 = 0.0799, wR_2 = 0.1976 for all data. Goodness-of-fit on F^2 = $\{\Sigma[w(F_o^2 - F_c^2)^2]/(n - p)\}^{1/2}$ = 1.082, where n is the number of reflections and p is the total number of parameters refined. All nonhydrogen atoms were refined anisotropically, and the hydrogen atoms were included in the final stages of the refinements on calculated positions bonded to their carrier atoms. The maximum/minimum residual electron density is 0.198/−0.231 e·Å^{-3}. Further details of the crystal structure investigations may be obtained from the Cambridge Crystallographic Data Centre [CCDC, 12 Union Road, Cambridge CB12 1 EZ (U.K.)] on quoting the depository number CCDC 781885.

2.2.2. DA-NPH (Phase II). $C_{15}H_{16}N_4O_2$, M_r = 284.3, monoclinic, space group Cc (point group m), a = 6.281(2) Å, b = 28.133(8) Å, c = 8.380(2) Å, β = 97.87(2)°, V = 1466.9(4) Å^3, Z = 4.[4]

2.3. Computational Details. All quantum chemical calculations were performed using the Gaussian 03 program[14] with the B3LYP hybrid functional[15] and the 6-311+G(d) basis set. The zero-frequency hyperpolarizabilities, β_{mnp}, were calculated by the finite field (FF) method as in ref 8 for the optimized molecular structures (OPT) as well as for the experimental structures (EXP) determined by the X-ray

single-crystal analysis. The molecular coordinate system xyz is here defined so that the molecular plane is along the yz plane and the direction of the ground-state dipole moment, $\boldsymbol{\mu}_g$, is parallel to the z-direction ($\boldsymbol{\mu}_g = -\boldsymbol{\mu}_z$). The $\boldsymbol{\beta}_{mnp}$ tensor components were calculated in this system and subsequently transformed to obtain the value and the direction of the maximal hyperpolarizability, $\boldsymbol{\beta}_{max}$ (i.e., the hyperpolarizability component along the main charge-transfer direction of the molecule). The effective hyperpolarizabilities, $\boldsymbol{\beta}_{ijk}^{eff}$ in the crystalline state were calculated by considering all projections of the hyperpolarizability tensor elements $\boldsymbol{\beta}_{mnp}$ of all molecules in the crystallographic system by the so-called oriented-gas model[16]

$$\boldsymbol{\beta}_{ijk}^{eff} = \frac{1}{n(g)} \sum_{s}^{n(g)} \sum_{mnp}^{3} \cos(\theta_{im}^s)\cos(\theta_{jn}^s)\cos(\theta_{kp}^s)\beta_{mnp} \quad (1)$$

where $n(g)$ is the number of equivalent positions in the unit cell, s denotes a site in the unit cell, and θ_{im}^s is the angle between the Cartesian axis i and the molecular axis m. In this model, the macroscopic susceptibility tensor elements, $\chi_{ijk}^{(2)}$, are related to the effective hyperpolarizabilities, $\boldsymbol{\beta}_{ijk}^{eff}$, as

$$\chi_{ijk}^{(2)} = NF_{ijk}\boldsymbol{\beta}_{ijk}^{eff} \quad (2)$$

where N is the number density of the molecules and F_{ijk} is the correction factor due to intermolecular interactions including the local-field corrections.

3. RESULTS AND DISCUSSION

3.1. Characteristics of NPH Derivatives. The chemical structures of the investigated NPH derivatives are shown in Figure 1. DA-NPH and DH-NPH (dihydroxybenzaldehyde-4-nitrophenylhydrazone) have a rod-shaped head, dimethylaminobenzaldehyde and dihydroxybenzaldehyde, respectively, while TMO-NPH has a disk-shaped head, trimethoxybenzaldehyde.

DA-NPH crystallizes in different polymorphic forms: form I with noncentrosymmetric, nonpolar space group $P2_12_12_1$, form II with noncentrosymmetric, polar space group Cc, and form III with centrosymmetric space group $P2_1/c$.[4b] In this work, we only consider the polymorph with substantial macroscopic second-order nonlinearity, which is the phase II polymorph crystallizing in the polar space group Cc.[4] In DA-NPH crystals (phase II), the hydrazone group, which acts as hydrogen bond donor site, is at the center of the molecule and the nitro group, which acts as hydrogen bond acceptor, is at the end of the molecule, as is most common for NPH derivatives.[4−8] Therefore, due to the position of the hydrogen bond donor and the acceptor sites, combined with the specific shape of DA-NPH molecules, they form a λ-shaped packing with a relatively large angle (>90°) between the neighboring molecules (see Figure 2), rather than head-to-tail hydrogen bonds.[4,5] In order to evaluate the relation between the molecular packing in the crystalline system and the macroscopic nonlinearity of DA-NPH crystals, we calculated the zero-frequency hyperpolarizability tensor, $\boldsymbol{\beta}_{ijk}$, of the DA-NPH (EXP) molecule by quantum chemical calculation with the finite-field density functional theory (FF-DFT) method, as well as the amplitude and the direction of the maximal first-order hyperpolarizability, $\boldsymbol{\beta}_{max}$, of the molecule in the crystalline system. In Figure 2, the dotted and the solid vectors present the directions of the polar axis of the crystal and the maximum first hyperpolarizability, $\boldsymbol{\beta}_{max}$, of the molecules as determined by finite-field calculations. The angle between the polar axis of the crystal and the hyperpolarizabilities $\boldsymbol{\beta}_{max}$ of DA-NPH molecules is relatively large, $\theta_p = 46.6°$, which leads to a relatively small order

parameter, $\cos^3(\theta_p) = 0.33$, which is still far from the optimal molecular packing with $\cos^3(\theta_p) = 1$ for optimizing the diagonal susceptibility element along the polar axis of the crystal.

A different hydrazone derivative, DH-NPH, was developed to improve the molecular packing of NPH derivatives for quadratic nonlinear optics (see Figure 1a).[12] For DH-NPH, the space-filling characteristics of the constituting molecules are similar to those of DA-NPH, but different functional groups alter the main intermolecular interactions common for DA-NPH and many other NPH derivatives. DH-NPH molecules have a rod-shaped head like DA-NPH, but the strong hydrogen bond donor site OH group at the opposite end of the nitro-group hydrogen bond acceptor site leads to strong head-to-tail hydrogen bonds in the crystal, resulting in a favorable acentric molecular packing with high order parameter, $\cos^3(\theta_p) = 0.80$.[17]

For achieving an improved molecular packing, we choose here another approach: we keep the main intermolecular interactions of DA-NPH and many other NPH derivatives and modify the space-filling characteristics using a different headgroup, disk-shaped trimethoxybenzaldehyde (see Figure 1b). The investigated TMO-NPH materials were prepared according to ref 12. For comparison, we also prepared DA-NPH crystals, whose optical and nonlinear optical properties were previously fully characterized.[4,10] The high purity of investigated materials was confirmed by ^{1}H NMR and elemental analysis. DA-NPH (phase II) noncentrosymmetric monoclinic crystals (see Figure 2) having a red-greenish prism morphology were obtained by the rapid cooling method in acetonitrile solution.

The chemical and physical characteristic data including the melting temperature, T_m, decomposition temperature, T_d, the maximal first-order hyperpolarizability, $\boldsymbol{\beta}_{max}$, the order parameter $\cos^3(\theta_p)$, and the effective hyperpolarizability tensor, $\boldsymbol{\beta}_{ijk}^{eff}$, are listed in Table 1. In different solvents, the wavelength of maximum absorption, λ_{max}, of TMO-NPH is similar: 408 nm in acetone, 403 nm in acetonitrile, and 403 nm in methanol solution. This means that the trimethoxybenzaldehyde head is not very sensitive to the environmental conditions, like the phenolic head of DH-NPH molecules.[17] The wavelength of maximum absorption λ_{max} for TMO-NPH (408 nm) is however lower than that for DA-NPH (430 nm) in acetone solution. According to the nonlinearity−transparency trade-off,[1] the molecular nonlinearity of TMO-NPH may be smaller than that of DA-NPH, which has been confirmed by quantum chemical calculation. As listed in Table 1, the maximal first-order hyperpolarizability, $\boldsymbol{\beta}_{max}$, of TMO-NPH (OPT) is about 57% that of DA-NPH (OPT).

The thermal properties including the melting temperature, T_m, and the decomposition temperature, T_d, were determined by differential scanning calorimetry (DSC) for a heating rate of 10 °C/min. The T_m and T_d were chosen at the peak position and the initial exothermic position, respectively, in the DSC thermodiagram. Figure 3 shows the DSC curves of TMO-NPH and DA-NPH(II) crystalline powders. Compared with DA-NPH, TMO-NPH exhibits a higher thermal stability with a higher T_d (220 °C for TMO-NPH and 193 °C for DA-NPH).

3.2. Single-Crystal Structures. In order to choose an appropriate solvent for the growth of single crystals, we measured the solubility of TMO-NPH crystals in various solvents. We kept the solutions with excessive amounts of crystalline powders for 3 days in an oven at 32 °C and then measured the amount of the dissolved powder. We determined the following solubilities of TMO-NPH: 2.6 g/100 g acetone, 1.2 g/100 g acetonitrile, and

3051

dx.doi.org/10.1021/cg200320f |*Cryst. Growth Des.* 2011, 11, 3049–3055

Table 1. Chemical and Physical Properties of NPH Derivatives. [a]

	λ_{max} (nm)	T_m (°C)	T_d (°C)	β_{max}(OPT) $(10^{-30}$ esu)	β_{max}(EXP) $(10^{-30}$ esu)	θ_p(EXP) (deg)	order parameter, $\cos^3(\theta_p)$	β_{ijk}^{eff} $(10^{-30}$ esu)
TMO-NPH	408	203	220	79.5	72.2	14.8	0.90	$\beta_{111}^{eff} = 65.2$; $\beta_{221}^{eff} = 4.6$
DA-NPH (II)	430	189	193	138.6	144.7	46.6	0.33	$\beta_{111}^{eff} = 50.9$; $\beta_{221}^{eff} = 50.2$

[a] The melting temperature, T_m, and the decomposition temperature, T_d, are determined by the peak position and the initial exothermic position, respectively, in the DSC thermodiagram. The maximal first-order hyperpolarizability, β_{max}, is determined by quantum chemical calculations with B3LYP/6-311+G* of optimized (OPT) and experimental (EXP) molecules. The angle θ_p is the angle between the polar axis of the crystalline system and the maximal first-order hyperpolarizabilities, β_{max} (charge-transfer direction), of the molecules. The highest diagonal and the highest off-diagonal effective hyperpolarizability tensor elements, $\beta_{ijk}^{eff} \propto \chi_{ijk}^{(2)}$, were calculated from the hyperpolarizability tensor components β_{mnp} of all molecules by considering their orientation in the crystallographic system. λ_{max} is the wavelength of the maximum absorption in acetone solution.

0.4 g/100 g methanol. We chose acetone solvent for the single-crystal growth.

For single-crystal structural analysis, TMO-NPH single crystals were grown by the slow evaporation method at 32 °C in acetone solution. TMO-NPH crystals obtained have the monoclinic Pn space group symmetry (point group symmetry m). Figure 4 shows the experimental molecular structure (EXP) of the TMO-NPH molecule in the crystalline state and the crystal-packing diagram of TMO-NPH crystals. In the crystals, TMO-NPH (EXP) molecule has a planar conformation as shown in Figure 4a. However, the planarity of the TMO-NPH molecule is not perfect: the trimethoxybenzaldehyde head is slightly out of the plane of the nitrophenylhydrazone with a small dihedral angle between the two phenyl rings of 13°. Large dihedral angle between the two aromatic (or heteroaromatic) rings in NPH derivatives is often accompanied with a large change of the first hyperpolarizability of the molecules with respect to the perfectly planar conformation, which is usually the case of optimized (OPT) molecules obtained by quantum chemical calculations.[8,17] In finite-field calculations, the maximal first-order hyperpolarizability, β_{max}, of TMO-NPH (EXP) is similar to that of TMO-NPH (OPT) with the planar conformation, as listed in Table 1, indicating that a small dihedral angle does not considerably alter the molecular nonlinearity in case of TMO-NPH.

The main supramolecular interactions between the TMO-NPH molecules in the crystalline state are strong hydrogen bonds between the hydrazone and the nitro groups, $N(2)$-$H \cdots O(2)-N(1)$ with $O \cdots H$ distances of about 2.3 Å and $C(7)$-$H \cdots O(2)-N(1)$ with $O \cdots H$ distances of about 2.4 Å, and form an acentric λ-shaped packing (i.e., polar acentric layer), as is characteristic for DA-NPH as well as many other NPH derivatives[4−8] (see Figure 4b). The polar acentric layers are stacked one by one with strong hydrogen bonds between the closest methoxy groups in the upper and the lower layer, $O-CH_3 \cdots O-CH_3$ with $O \cdots H$ distances of about 2.4, 2.7, and 2.8 Å, as shown in Figure 4c.

The number density of TMO-NPH molecules in the crystalline state is due to the larger size of the molecule, about 5% lower than that of DA-NPH. However, TMO-NPH molecules are packed more closely than DA-NPH molecules without any residual void in the crystalline state (cell volume 774.9 Å^3 and predicted volume based on van der Waals radii 801.3 Å^3 for TMO-NPH; cell volume 1466.8 Å^3 and predicted volume based on van der Waals radii 1437.2 Å^3 for DA-NPH),[18] which is due to the strong hydrogen bonds and the shape of the head. As commented earlier, molecular packing in the crystalline state could be changed by two strong factors, the intermolecular interactions and the space filling characteristics.
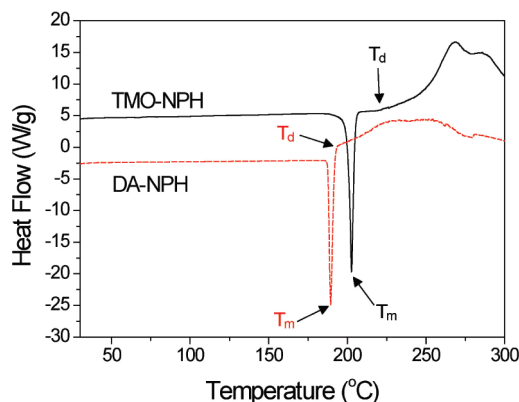
Figure 3. DSC curves of TMO-NPH and DA-NPH(II) crystalline powders showing T_m and T_d.

The most important difference in the molecular packing of TMO-NPH crystals compared with DA-NPH crystals is a much better parallel alignment of the NPH unit, which is essential for the nonlinear optical properties. In order to clearly determine the direction of the charge transfer in the crystalline state, we calculated the direction of the maximal first-order hyperpolarizability, β_{max}, of TMO-NPH (EXP) by quantum chemical calculation, which is illustrated in Figure 5. The dotted and the solid vectors present the direction of the polar axis of the crystal and β_{max} of the molecules, respectively. An acentric polar chain is oriented along the crystallographic c-axis, which is approximately (about 6° off in the ac crystallographic plane) along the polar axis of TMO-NPH crystals. The angle between the polar axis of the crystal and β_{max} of the molecules is $\theta_p \approx 14.8°$. Therefore, TMO-NPH crystals have an almost optimal molecular packing with a very high order parameter $\cos^3(\theta_p) = 0.90$ for quadratic nonlinear optical applications, which is considerably larger than that for DA-NPH crystals with a relatively low order parameter $\cos^3(\theta_p) = 0.33$. Therefore, even though the molecular nonlinearity is only half of that for DA-NPH crystals, TMO-NPH crystals can be expected to exhibit a large macroscopic nonlinearity, as discussed in the following section.

3.3. Macroscopic Nonlinearity with Optimal Molecular Packing. The macroscopic nonlinear optical properties of NPH crystals have been evaluated theoretically by calculating the effective hyperpolarizability tensor, $\beta_{ijk}^{eff} \propto \chi_{ijk}^{(2)}$ in the crystallographic system[8] and experimentally by the powder second harmonic generation (SHG) experiment[19] at a nonresonant fundamental wavelength of 1.9 μm.
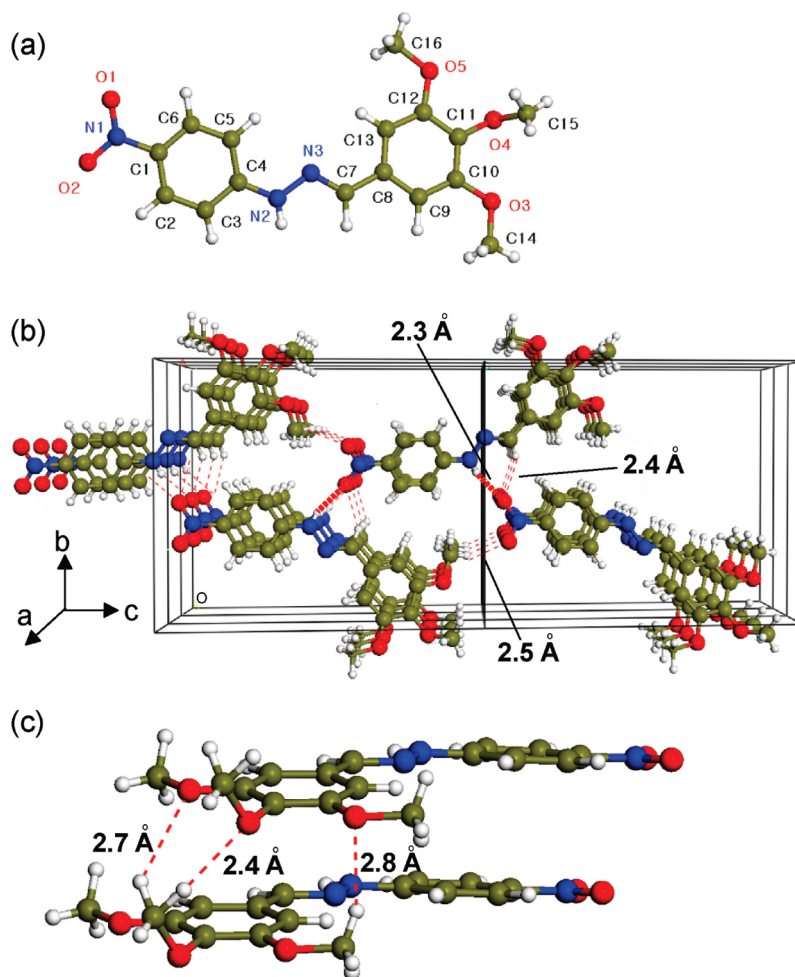
Figure 4. (a) Molecular structure of TMO-NPH molecule in the crystalline state, (b) crystal packing diagram of TMO-NPH crystals (the main supramolecular interactions between the molecules are strong hydrogen bonds of $N-O(2)\cdots H-N(2)$ with $O\cdots H$ distances of about 2.3 Å, which are presented by the thick dotted lines; selected weak hydrogen bonds are presented with the thin dotted lines), and (c) schematic illustration of the interlayer hydrogen-bond interactions.
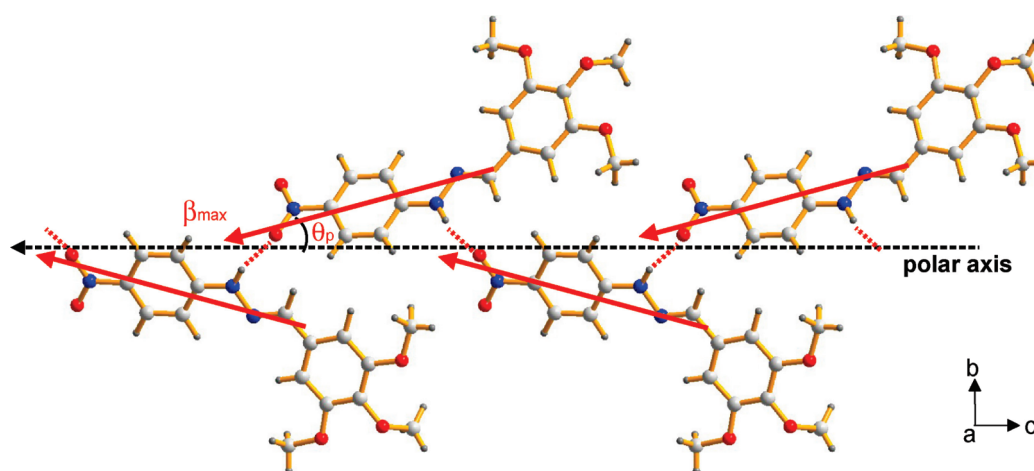
Figure 5. Schematic illustration of an acentric polar chain of TMO-NPH crystals projected along the *a*-axis. The solid and the dotted vectors present the directions of the maximum first hyperpolarizability, $\boldsymbol{\beta}_{max}$, as determined by finite-field calculations and the polar axis of the crystal, respectively. The angle between the polar axis of the crystal and the hyperpolarizabilities $\boldsymbol{\beta}_{max}$ of the molecules is $\theta_p \approx 14.8°$.

The effective hyperpolarizability tensor, $\boldsymbol{\beta}_{ijk}^{eff}$, was calculated according to eq 1 considering all hyperpolarizability tensor components $\boldsymbol{\beta}_{mnp}$ calculated by the finite-field method of the EXP molecules and the orientation of the molecules in the

crystal.[8] The resulting highest diagonal and off-diagonal effective hyperpolarizability tensor elements, $\boldsymbol{\beta}_{ijk}^{\text{eff}}$, are listed in Table 1. The relative values of the largest effective hyperpolarizability elements for DA-NPH listed in Table 1 are very well correlated with the rigorous susceptibility measurements giving $\chi_{111}^{(2)}(-2\omega,\omega,\omega) = 280$ pm/V and $\chi_{221}^{(2)}(-2\omega,\omega,\omega) = 320$ pm/V at the nonresonant fundamental wavelength of 1.9 μm.[10] In the Cartesian coordinate system for TMO-NPH crystals, the axis 1 is along the polar axis of the crystal (about 6° from the crystallographic c axis) and the axis 2 is along the symmetry b axis. All other effective hyperpolarizability tensor elements of TMO-NPH crystals are very small and can be neglected. The diagonal component of TMO-NPH crystals ($\boldsymbol{\beta}_{111}^{\text{eff}} = 65.2 \times 10^{-30}$ esu) is 30% higher than the highest element of DA-NPH ($\beta_{111}^{\text{eff}} = 50.9 \times 10^{-30}$ esu), even though the molecular susceptibility for TMO-NPH is only about half that of DA-NPH. This is because of the more aligned packing of TMO-NPH molecules with a very high order parameter.

The macroscopic nonlinearities have been screened by the Kurtz and Perry second-harmonic powder test[19] using a non-resonant fundamental wavelength of 1.9 μm. The relative second-harmonic generation (SHG) efficiency of TMO-NPH and DA-NPH crystalline powder is $\eta_{\text{TMO-NPH}}^{\text{exp}} = 10\%$ and $\eta_{\text{DA-NPH}}^{\text{exp}} = 76\%$, respectively, relative to the powder of one of the best organic salts, DAST (N,N-dimethylamino-N′-methyl-stilbazolium p-toluenesulfonate).[20] The measured SHG efficiency of DA-NPH powder, despite the predicted lower diagonal coefficient, is higher because (i) it has a high diagonal $\boldsymbol{\beta}_{111}^{\text{eff}}$ and a similarly high off-diagonal component $\boldsymbol{\beta}_{221}^{\text{eff}}$ (see Table 1) and the off-diagonal components $\boldsymbol{\beta}_{221}^{\text{eff}}$ contribute additionally to the powder test result and (ii) the off-diagonal components $\boldsymbol{\beta}_{221}^{\text{eff}}$ contribute about 50% more to the powder test result than the diagonal components $\boldsymbol{\beta}_{111}^{\text{eff}}$.[19] We can to some extent quantify different contributions by considering that the measured powder SHG efficiency is proportional to the squared number density of the molecules and the squared effective hyperpolarizability components, averaged over all possible orientations, that is, $N^2\langle(\boldsymbol{\beta}^{\text{eff}})^2\rangle$.[19] The spatial average can be calculated from the $\boldsymbol{\beta}_{ijk}^{\text{eff}}$ components by taking into account the point-group symmetry of the particular crystal.[19] The values of $N^2\langle(\boldsymbol{\beta}^{\text{eff}})^2\rangle$ were normalized to the values for DAST calculated with the data of ref 21, which leads to the following values with respect to DAST: $\eta_{\text{TMO-NPH}}^{\text{theor}} = 29\%$ for TMO-NPH and $\eta_{\text{DA-NPH}}^{\text{theor}} = 73\%$ for DA-NPH, which for DA-NPH is in very good agreement with the measurements. A bit lower measured values for TMO-NPH may be due to other effects that were not considered in our estimate, for example, the local-field factors that scale with refractive indices as well as variations due to possible phase-matched interactions. The refractive indices are similarly high for DA-NPH and DAST[10,20] but are expected to be lower for TMO-NPH because of the lower polarizability of the molecule compared with DA-NPH.

4. CONCLUSIONS

We have investigated a novel nonlinear optical nitrophenylhydrazone crystal, 3,4,5-trimethoxybenzaldehyde-4-nitrophenylhydrazone (TMO-NPH). Compared with previously investigated acentric DA-NPH crystals having a rod-shaped head, the TMO-NPH molecule maintains the acentric intermolecular synton through hydrazone and nitro groups, but distinct space-filling characteristics due to a different shape of the head group, disk-shaped trimethoxybenzaldehyde. We have investigated and analyzed the crystal structure and its characteristics, as well as the details of the microscopic and the macroscopic nonlinear optical properties by quantum chemical calculations using density functional theory (DFT) and powder second-harmonic generation at nonresonant conditions. TMO-NPH crystals have the monoclinic space group symmetry Pn and exhibit a large macroscopic optical nonlinearity due to a highly aligned molecular packing with a very high order parameter, $\cos^3(\theta_p) = 0.90$, while DA-NPH crystals exhibit a lower order parameter, $\cos^3(\theta_p) = 0.33$. The diagonal effective hyperpolarizability tensor component of TMO-NPH crystals is 30% higher than the highest component of DA-NPH, even though the molecular susceptibility for TMO-NPH is only about half of that for DA-NPH. Therefore, TMO-NPH crystals are interesting materials for second-order nonlinear optical applications, for which a high diagonal susceptibility element is required, such as electro-optics and terahertz-wave generation.

■ AUTHOR INFORMATION

Corresponding Author
*E-mail: opilkwon@ajou.ac.kr.

Present Addresses
†Korea Science Academy of KAIST, Busan 614-822, Korea.

■ REFERENCES

(1) (a) Jazbinsek, M.; Kwon, O. P.; Bosshard, Ch.; Günter, P. In *Handbook of Organic Electronics and Photonics*; Nalwa, S. H., Ed.; American Scientific Publishers: Los Angeles, 2008; Chapter 1. (b) Bosshard, Ch.; Sutter, K.; Prêtre, Ph.; Hulliger, J.; Flörsheimer, M.; Kaatz, P.; Günter, P. *Organic Nonlinear Optical Materials* Advances in Nonlinear Optics, Vol. 1; Gordon and Breach Science Publishers: Langhorne, PA, 1995.

(2) Bosshard, Ch.; Bösch, M.; Liakatas, I.; Jäger, M.; Günter, P. In *Nonlinear Optical Effects and Materials*; Günter, P., Ed.; Springer-Verlag: Berlin, 2000; Chapter 3.

(3) (a) Dalton, L. R.; Sullivan, P.; Jen, A. K. Y. In *Handbook of Photonics*; Gupta, M. C., Ballato, J., Eds.; CRC Press: Boca Raton, FL, 2007. (b) Nalwa, H. S.; Watanabe, T.; Miyata, S. In *Nonlinear Optics of Organic Molecules and Polymers*; Nalwa, H. S., Miyata, S., Eds.; CRC Press: Boca Raton, FL, 1997; Chapter 4.

(4) (a) Serbutoviez, Ch; Bosshard, Ch.; Knopfle, G.; Wyss, P.; Pretre, P.; Günter, P.; Schenk, K.; Solari, E.; Chapuis, G. *Chem. Mater.* **1995**, 7, 1198. (b) Pan, F.; Bosshard, Ch.; Wong, M. S.; Serbutoviez, Ch.; Follonier, S.; Günter, P.; Schenk, K. *J. Cryst. Growth* **1996**, 165, 273.

(5) Wong, M. S.; Gramlich, V.; Boshard, Ch.; Günter, P. *J. Mater. Chem.* **1997**, 7, 2021.

(6) Pan, F.; Bosshard, Ch.; Wong, M. S.; Serbutoviez, Ch.; Schenk, K.; Gramlich, V.; Günter, P. *Chem. Mater.* **1997**, 9, 1328.

(7) Wong, M. S.; Meier, U.; Pan, F.; Gramlich, V.; Günter, P. *Adv. Mater.* **1996**, 8, 416.

(8) (a) Kwon, O. P.; Jazbinsek, M.; Yun, H.; Seo, J. I.; Kim, E. M.; Lee, Y. S.; Günter, P. *Cryst. Growth Des.* **2008**, 8, 4021. (b) Kwon, O. P.; Jazbinsek, M.; Seo, J. I.; Kim, P. J.; Yun, H.; Lee, Y. S.; Günter, P. *J. Phys. Chem. C* **2009**, 113, 15405.

(9) (a) Tonouchi, N. *Nat. Photonics* **2007**, *1*, 97. (b) Ferguson, B.; Zhang, X. C. *Nat. Mater.* **2002**, *1*, 26.

(10) Follonier, S.; Bosshard, Ch.; Meier, U.; Knopfle, G.; Serbutoviez, C.; Pan, F.; Günter, P. *J. Opt. Soc. Am. B* **1997**, *14*, 593.

(11) Figi, H.; Mutter, L.; Hunziker, Ch.; Jazbinsek, M.; Günter, P.; Coe, B. J. *J. Opt. Soc. Am. B* **2008**, *25*, 1786.

(12) Liakatas, I.; Wong, M. S.; Gramlich, V.; Günter, P. *Adv. Mater.* **1998**, *10*, 777.

(13) Sheldrick, G. M. SHELXTL Programs, Version 5.1, Bruker AXSGmbH, Karlsruhe, Germany, 1998.

(14) Frisch, M. J.; Trucks, G. W.; Schlegel, H. B.; Scuseria, G. E.; Robb, M. A.; Cheeseman, J. R.; Montgomery, J. A., Jr.; Vreven, T.; Kudin, K. N.; Burant, J. C.; Millam, J. M.; Iyengar, S. S.; Tomasi, J.; Barone, V.; Mennucci, B.; Cossi, M.; Scalmani, G.; Rega, N.; Petersson, G. A.; Nakatsuji, H.; Hada, M.; Ehara, M.; Toyota, K.; Fukuda, R.; Hasegawa, J.; Ishida, M.; Nakajima, T.; Honda, Y.; Kitao, O.; Nakai, H.; Klene, M.; Li, X.; Knox, J. E.; Hratchian, H. P.; Cross, J. B.; Bakken, V.; Adamo, C.; Jaramillo, J.; Gomperts, R.; Stratmann, R. E.; Yazyev, O.; Austin, A. J.; Cammi, R.; Pomelli, C.; Ochterski, J. W.; Ayala, P. Y.; Morokuma, K.; Voth, G. A.; Salvador, P.; Dannenberg, J. J.; Zakrzewski, V. G.; Dapprich, S.; Daniels, A. D.; Strain, M. C.; Farkas, O.; Malick, D. K.; Rabuck, A. D.; Raghavachari, K.; Foresman, J. B.; Ortiz, J. V.; Cui, Q.; Baboul, A. G.; Clifford, S.; Cioslowski, J.; Stefanov, B. B.; Liu, G.; Liashenko, A.; Piskorz, P.; Komaromi, I.; Martin, R. L.; Fox, D. J.; Keith, T.; Al-Laham, M. A.; Peng, C. Y.; Nanayakkara, A.; Challacombe, M.; Gill, P. M. W.; Johnson, B.; Chen, W.; Wong, M. W.; Gonzalez, C.; Pople, J. A. *Gaussian 03*, revision C.02; Gaussian, Inc.: Wallingford, CT, 2003.

(15) (a) Perdew, J. P. *Phys. Rev. B* **1986**, *33*, 8822. (b) Becke, A. D. *J. Chem. Phys.* **1993**, *98*, 5648.

(16) Zyss, J.; Oudar, J. L. *Phys. Rev. A* **1982**, *26*, 2028.

(17) Kwon, O. P.; Jazbinsek, M.; Seo, J. I.; Choi, E. Y.; Yun, H.; Brunner, F. D. J.; Günter, P.; Lee, Y. S. *J. Chem. Phys.* **2009**, *130*, No. 134708.

(18) Connolly surface representation was generated using Materials Studio. Materials Studio (version 4.3.0.0), Program for Molecular Modeling and Analysis; Accelrys Software Inc., 2008.

(19) Kurtz, S. K.; Perry, T. T. *J. Appl. Phys.* **1968**, *39*, 3798.

(20) (a) Marder, S. R.; Perry, J. W.; Schaefer, W. P. *Science* **1989**, *245*, 626. (b) Pan, F.; Knöpfle, G.; Bosshard, Ch.; Follonier, S.; Spreiter, R.; Wong, M. S.; Günter, P. *Appl. Phys. Lett.* **1996**, *69*, 13.

(21) Kim, P. J.; Jeong, J. H.; Jazbinsek, M.; Kwon, S. J.; Yun, H.; Kim, J. T.; Lee, Y. S.; Baek, I. H.; Rotermund, F.; Günter, P.; Kwon, O. P. *CrystEngComm* **2011**, *13*, 444.